

Received February 25, 2019, accepted March 18, 2019, date of publication March 25, 2019, date of current version April 15, 2019.

Digital Object Identifier 10.1109/ACCESS.2019.2907124

Design Wideband Differential Bandpass Filter Using Slotline Surface Plasmon Polaritons

HAIWEN LIU¹, (Senior Member, IEEE), ZHENGBIAO WANG², (Student Member, IEEE),
QINGFENG ZHANG³, (Senior Member, IEEE), HUIFENG MA⁴,
BAOPING REN², (Student Member, IEEE), AND PIN WEN¹, (Student Member, IEEE)

¹School of Electronic and Information Engineering, Xi'an Jiaotong University, Xi'an 710049, China

²School of Information Engineering, East China Jiaotong University, Nanchang 330013, China

³Department of Electronic and Electrical Engineering, Southern University of Science and Technology, Shenzhen 518055, China

⁴School of Information Science and Engineering, Southeast University, Nanjing 210096, China

Corresponding author: Haiwen Liu (haiwen_liu@hotmail.com)

This work was supported in part by the National Science Foundation of China under Grant U1831201 and Grant 61461461020, in part by the Natural Science Foundation of Jiangxi Province under Grant 2017ACB20019, and in part by the Research Program of Jiangxi Province under Grant 2016BCB18010, Grant 20171BBE50056, and Grant 20181BCB24010.

ABSTRACT In this paper, a novel wideband differential bandpass filter (BPF) with slotline surface plasmon polaritons (SPPs) is proposed. It consists of a pair of differential microstrip-to-slotline transition, a slotline-to-SPP transition with subwavelength gradient grooves, and a slotline SPP waveguide, which supports the TEM, TE, and SPP modes, respectively. The dispersion and transmission characteristics of the proposed hybrid SPP structure are analyzed under differential-mode (DM) and common-mode (CM) operations and applied to design wideband differential filter. To validate the design concept, a filter sample has been designed, fabricated, and measured. Both simulated and measured results prove its good performance including a wide 3-dB fractional bandwidth of 147.6% centered at 4.2 GHz (f_0), a wide DM upper stopband to $4.8 f_0$ ($S_{21}^{dd} < -30$ dB), and a wide 40-dB CM suppression from 0.1 to 20 GHz.

INDEX TERMS Surface plasmon polariton (SPP), slotline, common/differential-mode, wideband, filter.

I. INTRODUCTION

As one of the most essential components in wireless communication systems, differential wideband bandpass filters (BPFs) have more advantages over the unbalanced ones, such as high data-rate transmissions, high immunity to the environmental noise and low electromagnetic interference. So, differential wideband BPFs with enhanced common-mode (CM) suppression and out-of-band differential-mode (DM) rejection have attracted tremendous attention in recent years. Up to now, many efforts have been paid to design differential wideband BPFs with good performance [1]–[16].

In [1], [2], two compact differential wideband BPFs with wide DM passband have been proposed based on branch-line structures. However, their CM rejections were limited to a frequency range slightly wider than the differential passband. In [3], T-shaped structures were used to achieve wideband harmonic suppression for the common mode. However, due

to the centrally loaded stub is shared by its CM and DM circuit models, the CM signals could not be perfectly suppressed in the DM passband of interest. Other wideband differential BPFs with different configurations were reported by using parallel coupled lines [4], modified coupled feed-lines [5], and ring resonators [6], [7]. Although wide DM passband can be achieved, the CM rejection of these filters during the DM passband are relatively poor.

To enhance the suppression of the CM signal, the transversal signal-interference technique was applied to design differential wideband BPFs [8]–[10]. However, the differential output/input ports of the differential filters in [8] are located on the opposite positions, which could not satisfy the requirement of practical applications. And the enhanced CM rejection of the differential filters in [9], [10] is obtained at a cost of large insertion loss. Other approaches, such as cross-shaped resonator [11], 180° phase shifters [12], and internal coupling technique [13] were also used to obtain deep CM rejection. However, poor DM selectivity were presented in these filters. In [14]–[16], EBG structure [14] and

The associate editor coordinating the review of this manuscript and approving it for publication was Feng Lin.

double-sided parallel strip [15], [16] were applied to improve the CM suppression respectively. However, the upper DM stopbands of these filters are a little narrow, and the circuits size are also somehow too large due to the usage of wideband transitions and periodic structure.

Recently, based on microstrip-to-slotline transitions, a novel class of differential filter with inherent CM suppression has been proposed [17]–[19]. By directly feeding the slotline resonator through the orthogonally placed microstrip line, the CM signal could be inherently suppressed along the slotline due to its high attenuation caused by filed mismatching. However, the filter proposed in [18] suffers from narrow DM upper stopband and poor selectivity, and the multi-layered filters reported in [19] is complicated with time-consuming optimization. In all, the research of the differential wideband BPFs is in progress, but still restricted.

Surface plasmon polaritons (SPPs) are intensely localized surface modes which propagate along the metal /dielectric interface. Due to the characteristics of high field confinement in a subwavelength scale, SPP waveguide research becomes an interesting field. Using the high confinement characteristics, single-sided and double-side slow-wave transmission lines with low ohmic losses are proposed based on SPP waveguides in [20], [21], respectively. In [22], a multi-layer SPP waveguide with a loadable space for active controlling elements has been proposed. In [23], a single-ended wideband BPFs with low radiation loss has been presented based on hybrid SIW-SPP transmission lines. In [24], based on asymmetric SIRs and SPP feeding structure, we proposed a balanced filter with a narrow single band. However, all these transmission lines, waveguides and filters are based on microstrip line or SIW technology. To the best of our knowledge, there is little study on the slotline SPP waveguide for differential circuit and component design.

In this paper, a microstrip-to-slotline transition and a slotline SPP waveguide are proposed. The slotline SPP waveguide has low-pass and slow-wave features, while the microstrip-to-slotline is a high-pass structure with intrinsic CM rejection characteristic. By bridging these two parts with a slotline-to-SPP transition, a novel wideband differential BPF with enhanced CM suppression and upper DM stopband is developed. The remainder of this paper is organized as follows. In Section II, the configuration of the proposed filter is presented, the operating principle is explained, and the design procedure is demonstrated. Then, a wideband differential BPF prototype was fabricated and measured. The simulated and measured results are displayed and discussed in Section III. Besides, comparison with some advanced works is also summarized in Section III. Finally, a brief conclusion is made in Section IV.

II. FILTER DESIGN

A. FILTER CONFIGURATION

The configuration of the proposed wideband differential BPF is shown in Fig. 1, which is ideally symmetric with respect

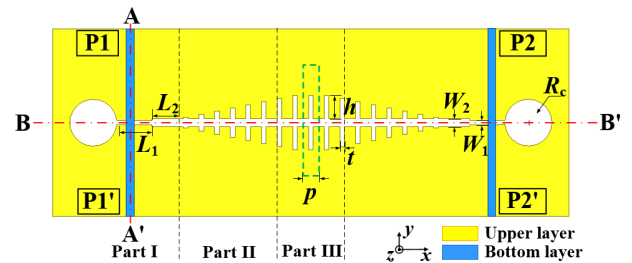


FIGURE 1. Schematic of the proposed filter. The microstrip feeding line is on blue bottom layer whereas the metal ground with slotline and SPP waveguide are on the yellow upper layer. Physical dimensions: $L_1 = 4.5$, $L_2 = 4$, $W_1 = 0.76$, $W_2 = 0.96$, $p = 2$, $h = 4$, $t = 0.4$, $R_c = 4$ (unit: mm).

to both xoz and yoz planes. A microstrip feeding-line with two differential ports (ports P1 and P1') are directly tapped on the slotline as input terminals while a mirror and feeding-line structure with two differential ports (P2 and P2') along yoz plane is placed as output terminals. A longitudinal slotline is etched on the ground plane, which can provide a mode conversion from slotline to SPP waveguide. To further understand the operating principle of the proposed filter, it is divided into three parts in Fig.1. Part I: Along the AA' cross plane of the microstrip-to-slotline transition, it provides signal transition from TEM-mode to TE-mode conversion. Part II: Along the BB' cross plane of the slotline-to-SPP transition, it is from TE-mode to SPP-mode conversion. Part III: There is slotline SPP waveguide with two series of sub-wavelength gradient grooves. In order to achieve a match of the momentum and the impedance between SPP waveguide and slotline in a wide frequency band, a transition with sub-wavelength gradient grooves is applied to bridge the groove line and the SPP waveguide. Shown in Fig. 1, the groove depth varies from zero to h .

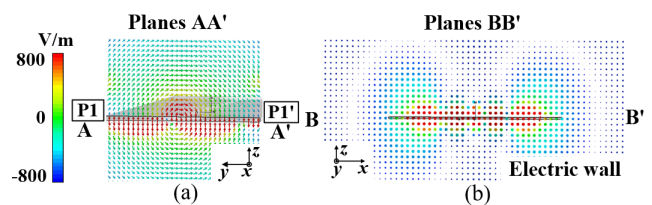


FIGURE 2. Electric field distributions of DM transmission on planes AA' and BB' at 7 GHz. (a) Electric field distributions on plane AA'. (b) Electric field distributions on plane BB'.

B. MICROSTRIP-TO-SLOTLINE TRANSITION

For the microstrip-to-slotline transition, its' boundary conditions on the symmetrical plane BB' are different under CM and DM excitation. By using this unique characteristic, an intrinsic CM rejection can be realized in the proposed filter. To further clarify the operating mechanism of the proposed microstrip-to-slotline transition, simulated electric field distributions on plane AA' and BB' under DM and CM excitation are displayed in Fig. 2 and Fig. 3 respectively.

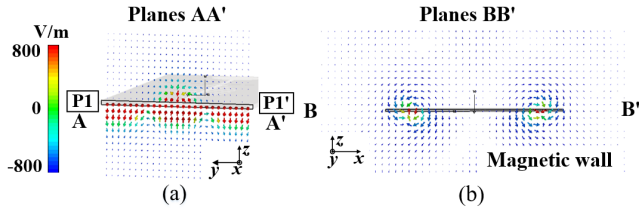


FIGURE 3. Electric field distributions of CM transmission on planes AA' and BB' at 7 GHz. (a) Electric field distributions on plane AA'. (b) Electric field distributions on plane BB'.

Under DM operation, the electric field excited in the microstrip feeding-line is perpendicular to the xoz plane, as shown in Figure 2(a). At the same time, the BB' plane (xoz plane) is used as a virtual electric wall, and the electric field that can propagate in the slotline is also perpendicular to the xoz plane, as shown in Fig. 2(b). Therefore, due to the similarity of the electric fields in the microstrip feeding-line and the slotline, it is highly desirable that the DM signal can be smoothly converted from the TEM mode (microstrip) to the TE mode (slot line).

While under CM operation, the symmetrical plane BB' plane (xoz plane) works like a virtual magnetic wall. In this situation, the electric field excited in the microstrip feeding line is parallel to the xoz plane, as shown in Fig. 3(a). However, the electric field which can propagate in the slotline is perpendicular to the xoz plane. That is, the electric field in the microstrip feeding line is orthogonal to that in the slotline. Hence, field mismatching will occur during the mode conversion, and the CM signal will be decayed along the slotline structure as shown in Fig. 3(b).

Besides the intrinsic CM suppression, the microstrip-to-slotline transition (Part I) is also a high-pass structure which provides a desired lower cutoff frequency f_L of the proposed differential filter. Once the specifications of substrate and f_L are determined, the radius of the circular slotline stubs R_c are chosen to achieve the lower cutoff frequency f_L . Since the radiation loss of the circular slotline stub increases with the circular slotline stubs gradually turn into radiating structures as frequency increases, and finally operate as radiating elements at the upper cutoff frequency f_U . Therefore, the radiation loss of the circular slotline stub increases with increasing frequency, and the choice of f_L will introduce restriction on the upper cutoff frequency f_U . Assuming that R_c is a quarter of the effective guidewave length of the slotline at f_U , an estimate for R_c can be expressed as:

$$R_{c(mm)} = 72 / (r \times f_L(GHz) \times \sqrt{\epsilon_{eff}}) \quad (1)$$

where r represents the frequency ratio of the upper cutoff frequency f_U to f_L , and $\epsilon_{eff} \approx (\epsilon_r + 1)/2$. To achieve a relative wide bandwidth, r is set as 6.6 in this work.

In order to verify the effectiveness of equation (1), the transmission coefficients of the proposed microstrip-to-slotline transition are first obtained by connecting two identical transitions with uniform $\lambda_g/4$ slotline, as shown

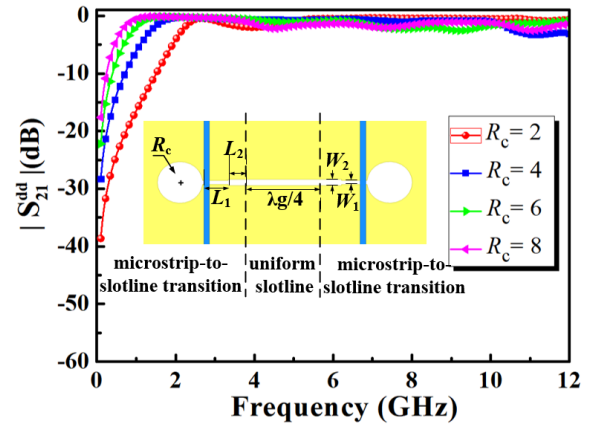


FIGURE 4. Simulated transmission coefficients of the proposed microstrip-to-slotline transitions with different R_c under DM excitation (the inset one are two proposed microstrip-to-slotline transitions connected by a uniform quarter wavelength slotlines).

in Fig. 4, where λ_g represents the guide wavelength at 6 GHz. As depicted in Fig. 4, the lower cutoff frequency of the microstrip-to-slotline transition is decreased from 2.4 to 0.6 GHz as R_c increased from 2 to 8 mm, which agree well with the predicted results of equation (1). Thus, the equation (1) can be applied to get the initial dimension of circular slotline stub. To further study the effect of R_c on the lower cutoff frequency of the proposed differential filter, the simulated coefficients of the proposed wideband differential BPF with different R_c under DM excitation are shown in Fig. 5. It is seen from Fig. 5 that the lower cutoff frequency f_L is changed from 1.3 to 0.6 GHz as R_c increases from 2 to 8mm. Thus, the lower cutoff frequency can be flexibly adjusted by R_c in a wide frequency range.

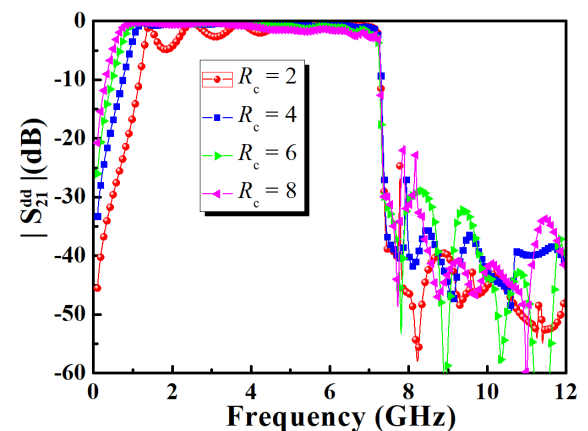


FIGURE 5. Simulated transmission coefficients of the proposed wideband differential BPF with different R_c under DM excitation (unit: mm).

C. SLOTLINE-TO-SPP TRANSITION AND SLOTLINE SPP WAVEGUIDE

For the slotline SPP waveguide (Part III), it's a slow-wave and low-pass structure which provides a desired upper cutoff

frequency of the proposed filter. To make a smooth III), a slotline-to-SPP transition (Part II) is applied to bridge mode conversion from TE mode (Part I) to SPP mode (Part these two parts, as shown in Fig. 1. For further understanding the operating principle of the Part II and Part III, the dispersion characteristics of SPP unit are analyzed by both theoretical and parametric studies. As presented in [25], when the copper thickness of the substrate is infinity, the dispersion curves for the SPP modes propagated in the metallic groove array can be expressed as:

$$\beta = \beta_0 \sqrt{1 + \frac{t^2}{p^2} \tan^2(\beta_0 h)} \quad (2)$$

where $\beta_0 = \omega/c$ represents the propagation constant of the EM waves in free space, p expresses the period of the unit cell, t and h represent the width and depth of the grooves. Due to the copper thickness of the substrate used in manufacturing is finite, a precise dispersion relation for the SPP modes propagated in Part II and Part III is analyzed by the *Eigenmode solver of commercial software CST Microwave Studio*, and the results are displayed in Fig. 6.

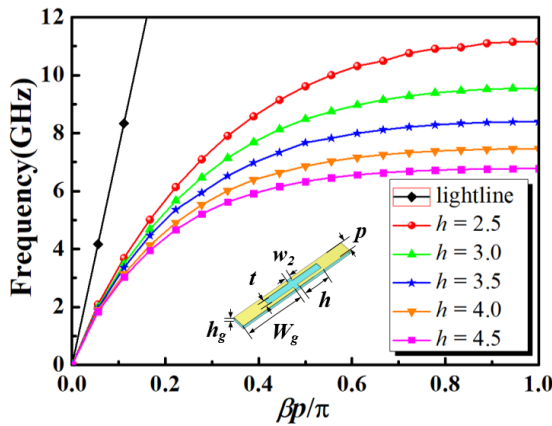


FIGURE 6. Dispersion curve of the proposed SPP unit cell in Part II and Part III. Dimensions of the SPP unit cell: $W_2 = 0.96$, $p = 2$, $t = 0.6$, $h_g = 0.635$, $W_g = 24$ (unit: mm).

As shown in Figure 6, the supported SPP mode is always below the lightline, which dedicates that the SPP mode is a kind of slow-wave. Therefore, the electromagnetic field will be tightly confined in the SPP waveguide without radiating into the space. Furthermore, at the same frequency, the propagation constant β of the SPP mode increases as the groove depth h increases, as displayed in Fig. 6. This not only means that the momentum matching can be achieved by the gradient grooves (varying from 0 to h) in Part II, but also means that the deeper the groove depth is, the tighter the electromagnetic field is confined. Besides, as depicted in Fig. 6, each of the dispersion curves tends to be horizontal and finally reach up to different cutoff frequencies as the groove depth h is changed. Thus, the upper cutoff frequency of the proposed filter can be adjusted flexibly by changing the groove depth h .

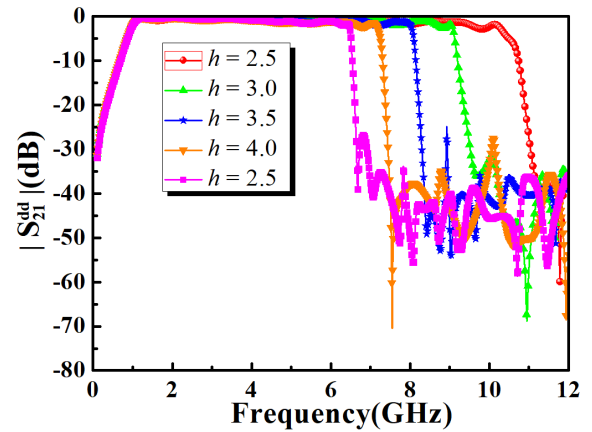


FIGURE 7. Simulated transmission coefficients of the proposed wideband differential BPF under DM excitation with different h (unit: mm).

The characteristics of controllable upper cutoff frequency is also verified by the simulated DM response shown in Fig. 7. As demonstrated in Fig. 7, the upper cutoff frequency of the proposed filter is decreased from 11.3 to 6.8 GHz as h increases from 2.5 to 4.5 mm. Hence, a BPF with desired center frequency $f_c = (f_U + f_L)/2$ and controllable bandwidth can be designed flexibly by choosing a proper combination of R_c and h . Moreover, as shown in Fig. 7, the insertion loss of the proposed filter varies from 0.28 to 2.3 dB across the DM passband, which is slightly larger than that of microstrip-to-slotline transition shown in Fig. 4 (varying from 0.1 to 2.2 dB). Thus, the insertion loss caused by the slotline SPP wave guide can be nearly ignored due to high confinement of SPP modes.

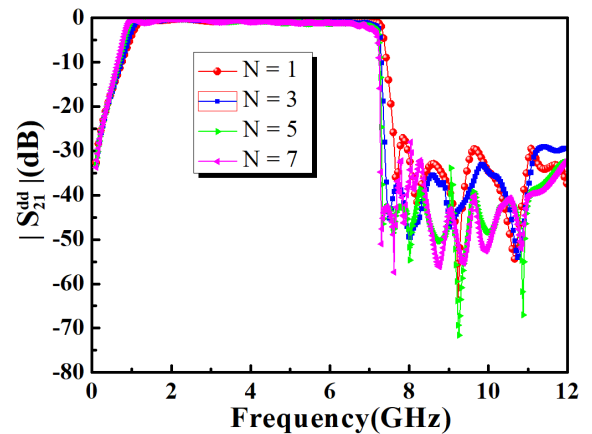


FIGURE 8. Simulated transmission coefficients of the proposed wideband differential BPF under DM excitation with different SPP unit cell numbers N .

In addition, the effect of different SPP unit number N on the proposed filter performance are displayed in Fig. 8. Results show that the upper sideband selectivity is improved greatly and the corresponding insertion loss is increased slightly as the number increases under DM operation. So, $N = 5$ is

chosen after a tradeoff between the frequency selectivity and the in-band insertion loss for the final design.

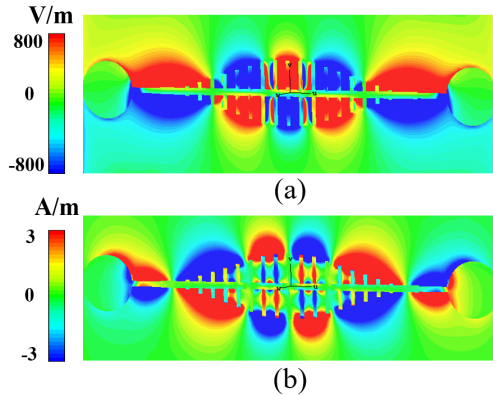


FIGURE 9. Simulated electric field and magnetic field distributions of the proposed wideband differential filter under DM excitation at 7 GHz (a) E_z -component. (b) H_y -component.

III. RESULTS AND DISCUSSIONS

To verify the above-mentioned analysis, a wideband differential BPF is designed and fabricated on a 0.635 mm thick Rogers 6010 substrate with a permittivity of 10.2 and loss tangent of 0.0023. The optimal dimension parameters are shown in Fig. 1 and the overall size of the proposed filter is $66 \times 20 \text{ mm}^2$. Fig. 9(a) and (b) show the simulated E_z electric field and H_y magnetic field distributions of the proposed filter under DM excitation. As shown in Fig. 9, the transversal fields of propagated SPP modes is well confined along the proposed slotline SPP waveguide, which means a low insertion loss can be achieved in the proposed filter. The simulated current distributions of the proposed filter under DM and CM excitation are displayed in Fig. 10(a) and (b) respectively.

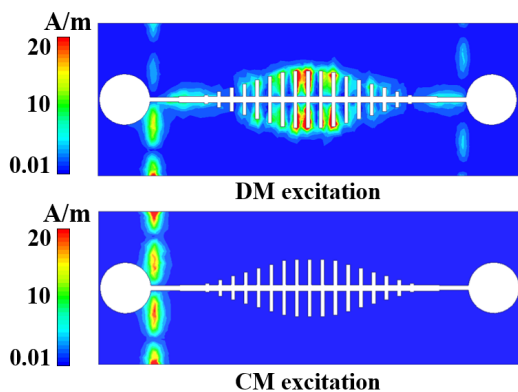


FIGURE 10. Simulated current distributions of the proposed wideband differential BPF under different excitation.

As shown in Fig. 10(a), under DM excitation, the DM signals can smoothly transmitted from microstrip feeding-line due to the successful TEM-to- TE mode version. Whereas under CM excitation, as shown in Fig. 10(b), the CM signals will decayed highly along the slotline due to the failure of mode

conversion caused by the filed mismatching, which is also agree well with the analysis demonstrated in Section II.

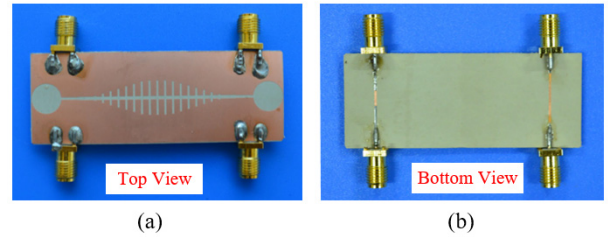


FIGURE 11. The photographs of the fabricated wideband differential BPF. (a)Top view. (b)Bottom view.

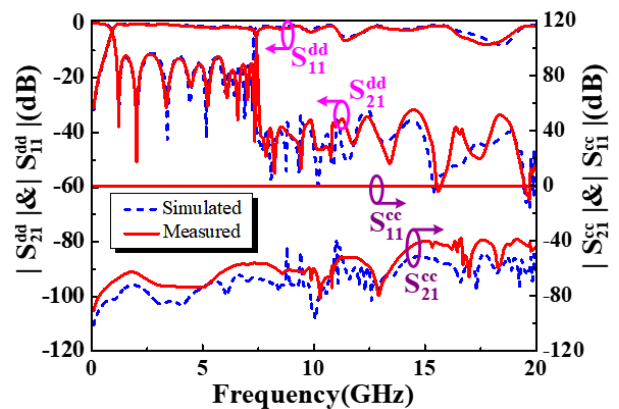


FIGURE 12. Simulated and measured S-parameters of the proposed wideband differential BPF.

The photographs of the fabricated wideband differential filter are shown in Fig. 11. Simulated and measured S-parameters are displayed and compared in Fig. 12. It is seen from Fig. 12 that the measured 3-dB DM fractional bandwidth of 147.6% from 1.1 to 7.3 GHz with the center frequency at $f_0 = 4.2 \text{ GHz}$ is produced, and the minimum insertion loss is of 0.28 dB at 2 GHz. The slightly increased insertion loss during the DM passband is mainly due to the enlarged radiation loss of circular slotline stubs with increasing frequency.

For the CM response, the measured CM signal rejection is lower than -55 dB within the DM passband and -40 dB from 0.1 to 20 GHz. Furthermore, the upper stopband of the proposed BPF under DM operation stretches up to $4.8f_0$ of 20 GHz ($S_{21}^{dd} < -30\text{dB}$). The ultra-wide upper stopband can be attributed to the wide band-gap existed between the fundamental SPP mode and higher-order SPP mode [26]. Besides, it can be found that the good DM transmission features and deep CM rejection displayed in Fig. 12 agree well with the current distributions shown in Fig. 10.

In addition, simulated and measured group delay of the proposed filter are shown Fig. 13. It can be observed from Fig. 13 that the group delay is less than 1ns from 1 to 7.3 GHz. The raised variation is caused by a trade-off between phase linearity and skirt rejection of the S_{21}^{dd} magnitude. In short,

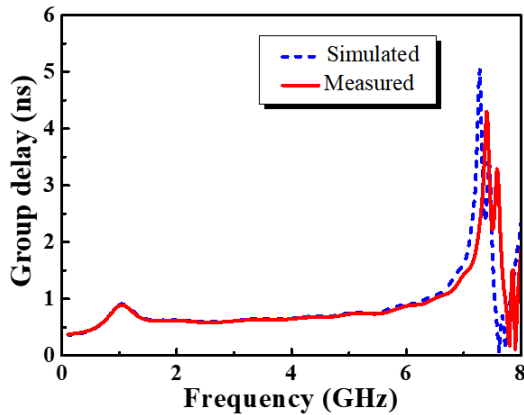


FIGURE 13. Simulated and measured group delay of the DM pass band of the proposed wideband differential BPF.

TABLE 1. Comparison with previous state-of-the-art differential wbpfs.

Ref	DM Performance				In-band CM Suppression	Size ($\lambda_g \times \lambda_g$)
	f_0 (GHz)	3-dB FBW	Maximum RL	Upper stopband S_{21}^{dB} (dB)		
[1]	6.5	119%	14.0 dB	< -15 (2.1 f_0)	9.6 dB	0.35×0.70
[2]	3.0	79%	10.0 dB	< -25 (2.6 f_0)	13 dB	0.51×0.51
[17]	3.6	105.5%	10.0 dB	< -15 (1.5 f_0)	47.5 dB	0.56×0.28
[18]	5.45	123.3%	9.8 dB	< -12 (2.6 f_0)	21.6 dB	0.39×0.19
[19]	4.25	115.0%	12.0 dB	< -20 (2.4 f_0)	20.0 dB	0.67×0.20
This work	4.2	147.6%	12.5 dB	< -30 (6 f_0)	55.0 dB	2.95×0.89

good agreement between the simulated and measured results verifies the effectiveness of this design. Table 1 further lists a comparison with other reported arts, which clearly shows the filter's enhanced bandwidths, upper stopband and good CM suppression.

IV. CONCLUSION

In this letter, a novel wideband differential BPF with enhanced CM suppression and a wide DM upper stopband is presented. Its microstrip-to-slotline and slotline-to-SPP transitions are designed and analyzed. Moreover, the dispersion and transmission characteristics of the proposed hybrid SPP structure are applied to design wideband differential filter. Results prove its good performance including a wide 3-dB fractional bandwidth of 147.6% centered at 4.2 GHz and a wider 40-dB CM suppression from 0.1 to 20 GHz. This novel slotline SPP structure is compact, high-performance and suitable for differential component design and subsystem design applications.

REFERENCES

- [1] T. B. Lim and L. Zhu, "A differential-mode wideband bandpass filter on microstrip line for UWB application," *IEEE Microw. Wireless Compon. Lett.*, vol. 19, no. 10, pp. 632–634, Oct. 2009.
- [2] T. B. Lim and L. Zhu, "Differential-mode ultra-wideband bandpass filter on microstrip line," *Electron. Lett.*, vol. 45, no. 22, pp. 1124–1125, Oct. 2009.
- [3] W. Feng and W. Che, "Novel wideband differential bandpass filters based on T-shaped structure," *IEEE Trans. Microw. Theory Techn.*, vol. 60, no. 6, pp. 1560–1568, Jun. 2012.
- [4] X.-H. Wu, Q.-X. Chu, and L.-L. Qiu, "Differential wideband bandpass filter with high-selectivity and common-mode suppression," *IEEE Microw. Wireless Compon. Lett.*, vol. 23, no. 12, pp. 644–646, Dec. 2013.
- [5] B. Zhang, Y. Wu, and Y. Liu, "Wideband single-ended and differential bandpass filters based on terminated coupled line structures," *IEEE Trans. Microw. Theory Techn.*, vol. 65, no. 3, pp. 761–774, Mar. 2017.
- [6] W. Feng, W. Che, Y. Ma, and Q. Xue, "Compact wideband differential bandpass filters using half-wavelength ring resonator," *IEEE Microw. Wireless Compon. Lett.*, vol. 23, no. 2, pp. 81–83, Feb. 2013.
- [7] W. Feng, W. Che, and Q. Xue, "Balanced filters with wideband common mode suppression using dual-mode ring resonators," *IEEE Trans. Circuits Syst. I, Reg. Papers*, vol. 62, no. 6, pp. 1499–1507, Jun. 2015.
- [8] H. T. Zhu, W. J. Feng, W. Q. Che, and Q. Xue, "Ultra-wideband differential bandpass filter based on transversal signal-interference concept," *Electron. Lett.*, vol. 47, no. 18, pp. 1033–1035, Sep. 2011.
- [9] S. Shi, W.-W. Choi, W. Che, K.-W. Tam, and Q. Xue, "Ultra-wideband differential bandpass filter with narrow notched band and improved common-mode suppression by DGS," *IEEE Microw. Wireless Compon. Lett.*, vol. 22, no. 4, pp. 185–187, Apr. 2012.
- [10] X.-H. Wu and Q.-X. Chu, "Compact differential ultra-wideband bandpass filter with common-mode suppression," *IEEE Microw. Wireless Compon. Lett.*, vol. 22, no. 9, pp. 456–458, Sep. 2012.
- [11] H. Wang, L. M. Gao, K. W. Tam, W. Kang, and W. Wu, "A wideband differential BPF with multiple differential- and common-mode transmission zeros using cross-shaped resonator," *IEEE Microw. Wireless Compon. Lett.*, vol. 24, no. 12, pp. 854–856, Dec. 2014.
- [12] X.-H. Wang, H. Zhang, and B.-Z. Wang, "A novel ultra-wideband differential filter based on microstrip line structures," *IEEE Microw. Wireless Compon. Lett.*, vol. 23, no. 3, pp. 128–130, Mar. 2013.
- [13] L. Li, J. Bao, J.-J. Du, and Y.-M. Wang, "Differential wideband bandpass filters with enhanced common-mode suppression using internal coupling technique," *IEEE Microw. Wireless Compon. Lett.*, vol. 24, no. 5, pp. 300–302, May 2014.
- [14] F. Martin, L. Zhu, J. Hong, and F. Medina, *Balanced Microwave Filters*. Hoboken, NJ, USA: Wiley, 2018.
- [15] X.-H. Wang, Q. Xue, and W.-W. Choi, "A novel ultra-wideband differential filter based on double-sided parallel-strip line," *IEEE Microw. Wireless Compon. Lett.*, vol. 20, no. 8, pp. 471–473, Aug. 2010.
- [16] W. J. Feng, W. Q. Che, T. F. Eibert, and Q. Xue, "Compact wideband differential bandpass filter based on the double-sided parallel-strip line and transversal signal-interaction concepts," *IET Microw., Antennas Propag.*, vol. 6, no. 2, pp. 186–195, Apr. 2012.
- [17] X. Guo, L. Zhu, K.-W. Tam, and W. Wu, "Wideband differential bandpass filters on multimode slotline resonator with intrinsic common-mode rejection," *IEEE Trans. Microw. Theory Techn.*, vol. 63, no. 5, pp. 1587–1594, May 2015.
- [18] Y.-J. Lu, S.-Y. Chen, and P. Hsu, "A differential-mode wideband bandpass filter with enhanced common-mode suppression using slotline resonator," *IEEE Microw. Wireless Compon. Lett.*, vol. 22, no. 10, pp. 503–505, Oct. 2012.
- [19] J. Shi, C. Shao, J.-X. Chen, Q.-Y. Lu, Y. Peng, and Z.-H. Bao, "Compact low-loss wideband differential bandpass filter with high common-mode suppression," *IEEE Microw. Wireless Compon. Lett.*, vol. 23, no. 9, pp. 480–482, Sep. 2013.
- [20] A. Kianinejad, Z. N. Chen, and C.-W. Qiu, "Design and modeling of spoof surface plasmon modes-based microwave slow-wave transmission line," *IEEE Trans. Microw. Theory Techn.*, vol. 63, no. 6, pp. 1817–1825, Jun. 2015.
- [21] A. Kianinejad, Z. N. Chen, and C.-W. Qiu, "Low-loss spoof surface plasmon slow-wave transmission lines with compact transition and high isolation," *IEEE Trans. Microw. Theory Techn.*, vol. 64, no. 10, pp. 3078–3086, Oct. 2016.
- [22] P. H. He, H. C. Zhang, W. X. Tang, Z. X. Wang, R. T. Yan, and T. J. Cui, "A multi-layer spoof surface plasmon polariton waveguide with corrugated ground," *IEEE Access*, vol. 5, pp. 25306–25311, 2017.
- [23] D.-F. Guan, P. You, Q. Zhang, K. Xiao, and S. W. Yong, "Hybrid spoof surface plasmon polariton and substrate integrated waveguide transmission line and its application in filter," *IEEE Trans. Microw. Theory Techn.*, vol. 65, no. 12, pp. 4925–4932, Dec. 2017.

- [24] H. Liu, T. Liu, Q. Zhang, B. Ren, and P. Wen, "Compact balanced bandpass filter design using asymmetric SIR pairs and spoof surface plasmon polariton feeding structure," *IEEE Microw. Wireless Compon. Lett.*, vol. 28, no. 11, pp. 987–989, Nov. 2018.
- [25] J. Y. Yin, H. C. Zhang, Y. Fan, and T. J. Cui, "Direct radiations of surface plasmon polariton waves by gradient groove depth and flaring metal structure," *IEEE Antennas Wireless Propag. Lett.*, vol. 15, pp. 865–868, 2015.
- [26] X. Liu, Y. Feng, B. Zhu, J. Zhao, and T. Jiang, "High-order modes of spoof surface plasmonic wave transmission on thin metal film structure," *Opt. Express*, vol. 21, no. 25, pp. 31155–31165, 2013.

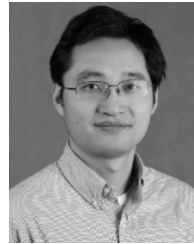


HAIWEN LIU (M'04–SM'13) received the B.S. degree in electronic system and the M.S. degree in radio physics from Wuhan University, Wuhan, China, in 1997 and 2000, respectively, and the Ph.D. degree in microwave engineering from Shanghai Jiao Tong University, Shanghai, China, in 2004.

From 2004 to 2006, he was a Research Assistant Professor with Waseda University, Kitakyushu, Japan. From 2006 to 2007, he was a Research Scientist with Kiel University, Kiel, Germany, granted by the Alexander von Humboldt Research Fellowship. From 2007 to 2008, he was a Professor with the Institute of Optics and Electronics, Chengdu, China, supported by the 100 Talents Program of Chinese Academy of Sciences. From 2009 to 2017, he was a Chair Professor with East China Jiaotong University, Nanchang, China. In 2014, he joined Duke University, Durham, NC, USA, as a Visiting Scholar. In 2015, he joined The University of Tokyo, Tokyo, as a Visiting Professor, supported by the JSPS Invitation Fellowship. In 2016, he joined the City University of Hong Kong, Hong Kong, as a Visiting Professor. Since 2017, he has been a Full-Time Professor with Xi'an Jiaotong University, Xi'an, China. He has authored or coauthored more than 100 papers in international and domestic journals and conferences. His current research interests include electromagnetic modeling of high-temperature superconducting circuits, RF and microwave passive circuits and systems, synthesis theory and practices of microwave filters and devices, antennas for wireless terminals, and radar systems. He was a recipient of the National Talent Plan, China, in 2017. He has served as the Editor-in-Chief for the *International Journal of RF and Microwave Computer-Aided Engineering* (Wiley), an Associate Editor for the *IEEE Access*, and the Guest Chief Editor for the *International Journal of Antennas and Propagation*. He was the Executive Chairman of the National Antenna Conference of China, in 2015, and a Co-Chairman of the National Compressive Sensing Workshop of China, in 2011, and the Communication Development Workshop of China, in 2016.



ZHENG BIAO WANG (S'16) received the B.S. degree in communication engineering from East China Jiaotong University, Nanchang, China, in 2016, where he is currently pursuing the M.S. degree in communication and information system. His current research interests include spoof surface plasmon polaritons and planar antennas for wireless communications.



QINGFENG ZHANG (S'07–M'11–SM'15) received the B.E. degree in electrical engineering from the University of Science and Technology of China, Hefei, China, in 2007, and the Ph.D. degree in electrical engineering from Nanyang Technological University, Singapore, in 2011. From 2011 to 2013, he was a Postdoctoral Fellow with the Poly-Grames Research Center, Ecole Polytechnique de Montreal, Montreal, QC, Canada. Since 2013, he has been an Assistant Professor with the Southern University of Science and Technology, Shenzhen, China. He has authored or coauthored more than 100 research papers. His current research interests include emerging novel electromagnetics technologies and multidisciplinary topics. He was a TPC Member of several international conferences including EUCAP 2015, APCAP 2015, and EUCAP 2017. He was a recipient of the Shenzhen Overseas High-Caliber Personnel, in 2014, the Guangdong Natural Science Funds for Distinguished Young Scholar, in 2015, the Shenzhen Nanshan Piloting Talents, in 2016, and the Guangdong Special Support Program for Top-Notch Young Talents, in 2017. He has been serving as an Associate Editor for the *IEEE Access*, since 2017, and was a Lead Guest Editor for the *International Journal Antennas and Propagation*, from 2014 to 2015. He was the Publication Chair of the IEEE ICCS, in 2016. He serves on the Review Board for several microwave journals.



HUI FENG MA received the B.S. degree in electronic engineering from the Nanjing University of Science and Technology, Nanjing, China, in 2004, and the Ph.D. degree from the State Key Laboratory of Millimeter Waves, Southeast University, Nanjing, in 2010. In 2010, he joined the School of Information Science and Engineering, Southeast University, Dhaka, Bangladesh, where he was promoted to an Associate Professor, in 2011, and a Full Professor, in 2015. His current research interests include metamaterial antennas, spoof surface plasmon polaritons, and other novel metamaterial functional devices including theoretical design and experimental realization. He was a recipient of the Second Prize of National Award for Natural Science, China, in 2014. He received the First Prize of Natural Science from the Ministry of Education, China, in 2011. His research of 3-D ground carpet cloak realized by using metamaterials has been selected as one of the 10 Breakthroughs of Chinese Science, in 2010.



BAOPING REN (S'16) received the B.S. degree in communication engineering and the M.S. degree in communication and information system from East China Jiaotong University, Nanchang, China, in 2011 and 2014, respectively. He is currently pursuing the Ph.D. degree in microwave engineering with Saitama University, Japan. In 2014, he became a Research Assistant with East China Jiaotong University. His current research interests include microwave circuits and devices, and high-temperature superconducting filters.



PIN WEN (S'16) received the B.S. degree in communication engineering and the M.S. degree in communication and information system from East China Jiaotong University, Nanchang, China, in 2012 and 2015, respectively. He is currently pursuing the Ph.D. degree in microwave engineering with Xi'an Jiaotong University, China. In 2015, he became a Research Assistant with East China Jiaotong University. His current research interests include antenna theory and design, and superconducting filter design.

...